



Cite this: DOI: 10.1039/d1cc05643c

Received 6th October 2021,
Accepted 22nd November 2021

DOI: 10.1039/d1cc05643c

rsc.li/chemcomm

Direct imaging of lattice planes in atomically precise noble metal cluster crystals using a conventional transmission electron microscope†

Ananthu Mahendranath,^{abc} Biswajit Mondal,^{ab} Korath Shivan Sugi^{ab} and Thalappil Pradeep^{id} *^{ab}

Imaging finer structural details of atomically precise noble metal cluster crystals has been difficult with electron microscopy, owing to their extreme beam sensitivity. Here we present a simple method whereby lattice planes in single crystals of nanoclusters can be observed using a conventional transmission electron microscope, enabling further expansion of cluster research.

Atomically precise noble metal clusters (APNMCs) belong to an emerging class of materials with unusual properties.^{1–3} Over one hundred nanocluster molecules have been understood with single crystal diffraction leading to their atomic structures.^{4–11} Consequently, the application of quantum chemical simulations has allowed us to unravel their spectroscopic properties.¹² A large number of other clusters are known today with their compositions being determined by advanced mass spectrometry.¹³ While spectroscopy,^{14,15} chemistry,^{16–18} catalysis,^{19,20} and applications^{21,22} of all of them are intensely pursued, absence of precise structures makes a thorough understanding of their properties difficult.

Single crystal diffraction, the preeminent tool for structural elucidation, requires high quality single crystals. While micro-crystal electron diffraction and single particle reconstruction coupled with computer modelling have revealed the structures of many molecules including clusters,^{23–26} they are still not commonly used in cluster science, excepting the report on Au₆₈.²⁴ The traditional transmission electron microscope (TEM), available in most of the research institutions, is generally not adequate for routine characterization of APNMCs and their crystals, in view of the extreme beam sensitivity of fragile

clusters, which transforms them to nanoparticles instantaneously upon electron beam exposure.²⁷ A method to observe clusters under such conditions for precise determination of their lattice parameters would facilitate the growth of cluster science.

In this communication, we present a simple way to image cluster crystals using a traditional transmission electron microscope where beam induced damage is minimized. Through this methodology, we have successfully imaged various lattice planes in three APNMCs

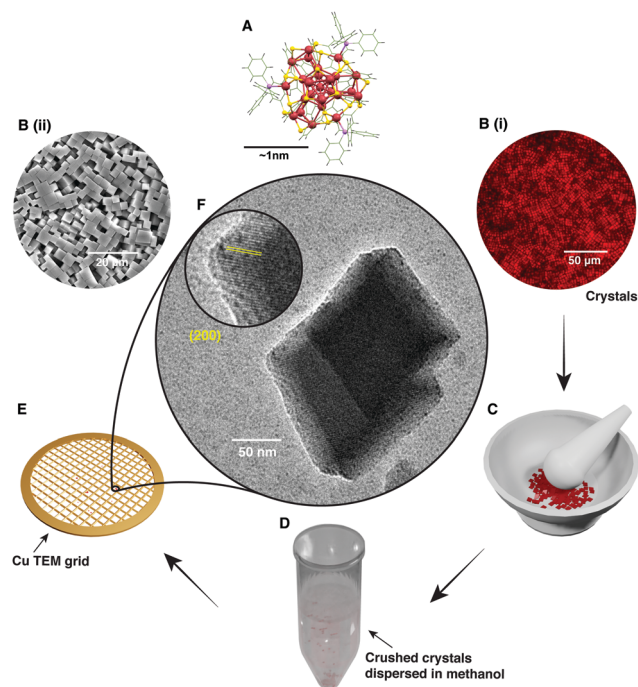


Fig. 1 (A) Single crystal X-ray structure of [Ag₂₉BDT₁₂TPP₄]³⁻ cluster. B(i) represent optical image and B(ii) SEM image of the as-crystallized Ag₂₉ crystals prepared by solvent evaporation. (C–E) Schematic of the process involved in sample preparation. (F) Shows TEM image of Ag₂₉C crystallites. Inset of (F) shows an expanded view of the (200) lattice plane of Ag₂₉C.

^a DST Unit of Nanoscience and Thematic Unit of Excellence, Department of Chemistry, Indian Institute of Technology Madras, Chennai 600036, India. E-mail: pradeep@iitm.ac.in

^b Centre of Excellence on Molecular Materials and Functions, Indian Institute of Technology Madras, Chennai, 600036, India

^c Department of Metallurgical and Materials Engineering, Indian Institute of Technology Madras, Chennai, 600036, India

† Electronic supplementary information (ESI) available. See DOI: 10.1039/d1cc05643c

whose structure has been solved previously using single crystal X-ray diffraction, namely – cubic (C) $[\text{Ag}_{29}(\text{BDT})_{12}(\text{TPP})_4]^{3-}$ (ref. 7), its trigonal (T) polymorph,²⁸ and $[\text{Ag}_{25}(\text{DMBT})_{18}]^-$ (ref. 9), where BDT, TPP, and DMBT are 1,3-benzenedithiol, triphenylphosphine, and 2,4-dimethylbenzenethiol, respectively. The method is schematically illustrated in Fig. 1 with $[\text{Ag}_{29}(\text{BDT})_{12}(\text{TPP})_4]^{3-}$ (abbreviated as Ag_{29}C , C refers to cubic polymorph) as a model. We start with Ag_{29}C single crystals of edge length varying from around 0.1 μm to 80 μm , which are routinely crystallized in the laboratory by solvent evaporation (see the experimental section in ESI† for further details). All the clusters discussed here were fully characterized using UV-Vis spectroscopy, and ESI MS (Fig. S1–S3, ESI†). Results were in agreement with the reported data. The single crystal morphology was as per literature and the structural parameters were checked with SCXRD (Tables S2 and S3, ESI†). About 100 such single crystals weighing around 0.5 mg were carefully transferred from a glass slide used for crystal growth and were ground thoroughly with a mortar and pestle, to make a powder composed of 0.02 μm to 0.7 μm particles (see ESI† Fig. S4, for further details and an optical micrograph of the powder). This cluster crystal powder was suspended in methanol, in which the cluster was insoluble, and was sonicated for 10 s. About 10 μl of this suspension was drop-casted on a carbon coated 300 mesh copper grid. After drying for 2 h, the sample was imaged under 100 kV electron beam

using a JEOL 3010 TEM, with a LaB_6 filament, having 1.2 Å point-to-point resolution. Cluster crystals were noticed immediately under the electron beam while continuous exposure of more than 60 s damages the crystals. This time may be used to optimize parameters for better imaging. By moving the beam to an adjacent crystal, it was possible to collect more than 10 images without beam induced damage.

While examining such crystallites, we observe the various lattice structures of Ag_{29}C , as shown in Fig. 2(A–C). These correspond to (110), (111), and (200) planes with lattice constants of 2.42 nm, 1.97 nm and 1.71 nm, respectively. Due to the cubic symmetry of Ag_{29}C , these may also correspond to equivalent planes in other directions (ESI† Table S4). Several other adjacent Ag_{29}C crystallites on the grid are also presented in the ESI† (Fig. S5). These lattice parameters match well with the crystallographic data reported by AbdulHalim, *et al.*⁸ We compare the TEM images with the crystal structures in Fig. 2(D–F).

Once beam induced damage sets in, nanoclusters coalesce to form larger nanoparticles. To understand the optimum time during which measurements can be done, before beam induced damages occur, we exposed the sample to the electron beam for an extended period of time. As mentioned previously, images can be collected for about 60 s from one crystallite,

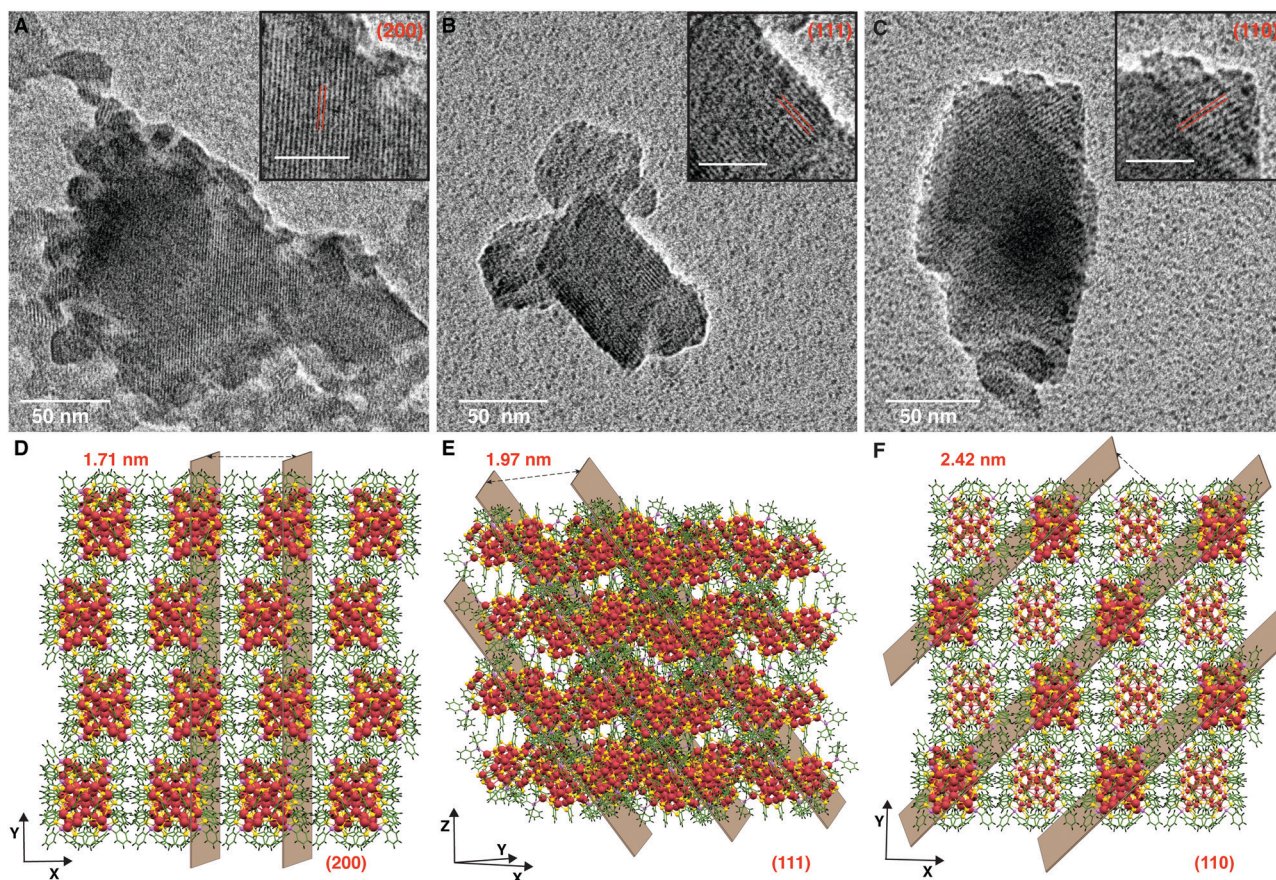


Fig. 2 TEM images of Ag_{29}C crystallites representing various lattice planes (A–C). The insets show expanded views of the corresponding lattice planes. (D–F) are representative images of a $2 \times 2 \times 2$ unit cell of Ag_{29}C . Scale bars in insets are 25 nm. Early signs of beam induced damage are seen in B.

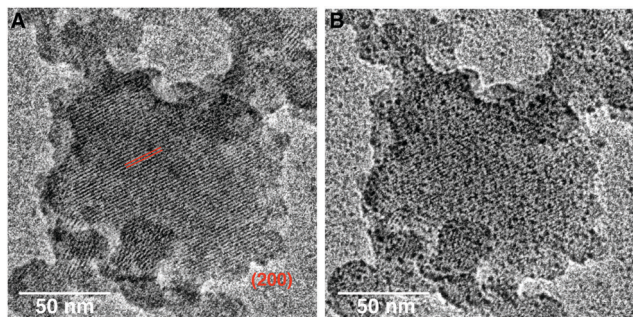


Fig. 3 (A) TEM image of an Ag_{29}C crystallite imaged without any noticeable damages. (B) Nanoparticle growth that happened over the region, after an exposure of nearly 56 s.

without noticeable beam induced damage, during which approximately 10 images could be collected for each area. However, beam induced damages set in the course of time and the lattice transforms continuously after 60 s. The systematic transformation is captured in ESI† (Fig. S6 and S8), and two of those images are presented in Fig. 3. As observed, beyond 60 s (Fig. S8, ESI†), the sample undergoes permanent changes and lattice planes are no more visible. Particles up to approximately 3.8 nm diameter were observed till 56 s (Fig. S7, ESI†). Bigger particles (> 10 nm) were formed up on exposure beyond ~2 min (Fig. S9, ESI†). It is to be noted that the direction of growth of these particles is not yet clear and is beyond the scope of experiments discussed here. In this

methodology, by reducing the accelerating voltage, we have managed to delay the damages happening to APNMCs. This creates a time window to image lattice planes, before beam induced damages become predominant. We believe that the success of this imaging methodology is also related to the thickness of the sample as well as the relative orientation of crystals on the TEM grid, with enhanced thermal contact with the grid. Therefore, removing those crystallites without proper contact by gentle tapping or inverting the grid, after drying the sample on the grid, can enhance the success of imaging. Improving thermal contact may be possible with grids such as ultra thin carbon film, microgrid, and those with supports such as molybdenum mesh and gold mesh. Thicker crystallites were opaque to electron beam (Fig. S10, ESI†). Note that images were collected at room temperature. When an acceleration potential greater than 100 kV was used, the crystallites got damaged sooner and the very first images showed signs of particle formation. With 100 kV voltage, all our attempts were successful in obtaining high quality images. The conditions used for imaging are presented as Table S1 in ESI†.

In order to ensure that this methodology is applicable for other crystals, we examined trigonal single crystals of $[\text{Ag}_{29}(\text{BDT})_{12}(\text{TPP})_4]^{3-}$ cluster (abbreviated as Ag_{29}T), which was a polymorph reported by our group.²⁸ The images correlated exactly to the single crystal structure of crystal of Ag_{29}T , as seen in Fig. 4(A–D). The lattice planes observed were (011) and (012) with interplanar spacings of 2.12 nm and 1.68 nm, respectively. Additional images from adjacent Ag_{29}T crystallites

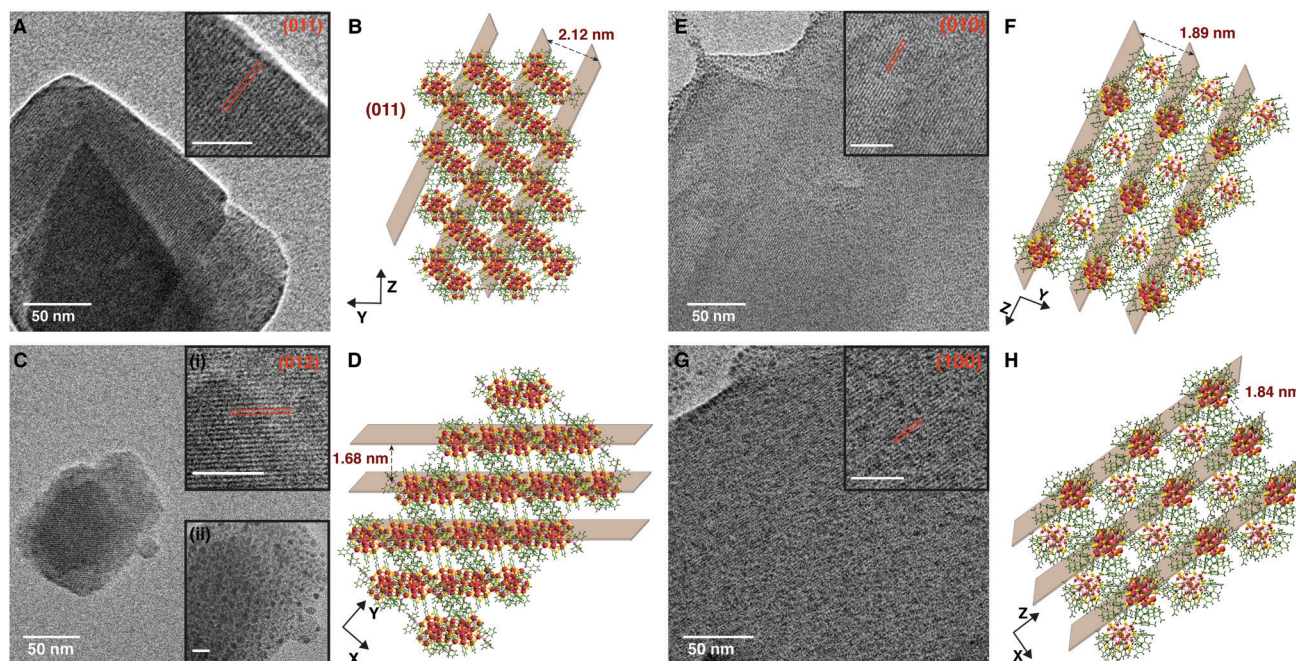


Fig. 4 TEM images of various crystallites representing different lattice planes of Ag_{29}T and Ag_{25} . (A and C) represent TEM images of Ag_{29}T crystallites and (B and D) are representative images of corresponding planes in a $2 \times 2 \times 2$ unit cell of the same crystal. Inset in A represents the expanded image of the crystallite. Insets (i and ii) show an expanded area of the crystallite and beam induced damage from another area after nearly 60 s of exposure. (E and G) represent TEM images from Ag_{25} crystallites and (F and H) are representative images of corresponding planes in a $3 \times 3 \times 3$ unit cell. Insets in (E and G) show expanded views of the crystallites. The scale bars in all insets are 25 nm, except for (ii), where it is 10 nm.

and beam induced damages on one of them are presented in ESI† as Fig. S11 and S12, respectively. Ag₂₉T shows beam induced damage after 60 s of beam exposure (Fig. C(ii)).

Furthermore, we observed single crystals of [Ag₂₅(DMBT)₁₈]⁻ (abbreviated as Ag₂₅) as well. The lattice spacings observed in these images were consistent with the expected distances in Ag₂₅ crystallites, which are triclinic, as depicted in Fig. 4(E–H). Additional images of the Ag₂₅ crystallites are presented as Fig. S13 (ESI†). Ag₂₅ also shows beam induced damage, as shown in the inset of Fig. 4G. As in the case of Ag₂₉C, the planes may correspond to equivalent ones in other directions, due to the trigonal and triclinic symmetries of Ag₂₉T and Ag₂₅, respectively (Tables S5–S6, ESI†).

We had also performed this experiment by using water as a solvent to disperse the cluster crystal powder. Both Ag₂₉C and Ag₂₉T are insoluble in water. While using water as a solvent, the grid was dried for an extended period of 6 h before imaging. Similar results were obtained and are presented as Fig. S14 in the ESI.† Detailed analysis followed for obtaining the lattice spacing in the crystallites, is described in ESI† (Tables S4–S6 and Fig. S15).

In conclusion, we show that a simple methodology can make cluster crystals observable with regular transmission electron microscopes available in most research laboratories. Generally, APNMCs grow in size and their structure gets transformed upon exposure to electron beam. We demonstrate that with careful sample preparation and optimized imaging parameters, finer structural details of nanocluster single crystals can be obtained, without causing damages, using electron microscope models that are employed for routine imaging. This will ensure more details of such fragile materials to be examined in many labs across the world. If this methodology were to be applied with improved instrumentation like low-dose imaging, cryo-cooling, etc., we anticipate that even the ligands will be observable. Consequently, we hope that crystal structures of unknown clusters will be determined more routinely.

A. M, thanks Ministry of Education, Government of India, and IIT Madras for his fellowship. We thank Ms. Jayoti Roy and Ms. Anagha Jose, for assisting with mass spectrometric analysis. T. P. acknowledges funding for the Centre of Excellence on Molecular Materials and Functions under the Institution of Eminence scheme of IIT Madras. We thank the Department of Science and Technology, Government of India, for supporting our research programme.

Conflicts of interest

There are no conflicts to declare.

References

- 1 I. Chakraborty and T. Pradeep, *Chem. Rev.*, 2017, **117**, 8208–8271.
- 2 R. Jin, C. Zeng, M. Zhou and Y. Chen, *Chem. Rev.*, 2016, **116**, 10346–10413.
- 3 X. Kang, Y. Li, M. Zhu and R. Jin, *Chem. Soc. Rev.*, 2020, **49**, 6443–6514.
- 4 P. D. Jadzinsky, G. Calero, C. J. Ackerson, D. A. Bushnell and R. D. Kornberg, *Science*, 2007, **318**, 430–433.
- 5 M. Bodiuzzaman, A. Ghosh, K. S. Sugi, A. Nag, E. Khatun, B. Varghese, G. Paramasivam, S. Antharjanam, G. Natarajan and T. Pradeep, *Angew. Chem., Int. Ed.*, 2019, **58**, 189–194.
- 6 D. Crasto, S. Malola, G. Brosofsky, A. Dass and H. Häkkinen, *J. Am. Chem. Soc.*, 2014, **136**, 5000–5005.
- 7 M. W. Heaven, A. Dass, P. S. White, K. M. Holt and R. W. Murray, *J. Am. Chem. Soc.*, 2008, **130**, 3754–3755.
- 8 L. G. AbdulHalim, M. S. Bootharaju, Q. Tang, S. Del Gobbo, R. G. AbdulHalim, M. Eddaoudi, D. Jiang and O. M. Bakr, *J. Am. Chem. Soc.*, 2015, **137**, 11970–11975.
- 9 Y. Li and R. Jin, *J. Am. Chem. Soc.*, 2020, **142**, 13627–13644.
- 10 C. P. Joshi, M. S. Bootharaju, M. J. Alhilaly and O. M. Bakr, *J. Am. Chem. Soc.*, 2015, **137**, 11578–11581.
- 11 S. Lee, M. S. Bootharaju, G. Deng, S. Malola, W. Baek, H. Häkkinen, N. Zheng and T. Hyeon, *J. Am. Chem. Soc.*, 2020, **142**, 13974–13981.
- 12 M. Zhu, C. M. Aikens, F. J. Hollander, G. C. Schatz and R. Jin, *J. Am. Chem. Soc.*, 2008, **130**, 5883–5885.
- 13 P. Chakraborty and T. Pradeep, *NPJ Asia Mater.*, 2019, **11**, 1–22.
- 14 Y. Lin, P. Charchar, A. J. Christofferson, M. R. Thomas, N. Todorova, M. M. Mazo, Q. Chen, J. Douth, R. Richardson, I. Yarovsky and M. M. Stevens, *J. Am. Chem. Soc.*, 2018, **140**, 18217–18226.
- 15 M. Neumaier, A. Baksi, P. Weis, E. K. Schneider, P. Chakraborty, H. Hahn, T. Pradeep and M. M. Kappes, *J. Am. Chem. Soc.*, 2021, **143**, 6969–6980.
- 16 K. R. Krishnadas, A. Ghosh, A. Baksi, I. Chakraborty, G. Natarajan and T. Pradeep, *J. Am. Chem. Soc.*, 2015, **138**, 140–148.
- 17 K. R. Krishnadas, A. Baksi, A. Ghosh, G. Natarajan, A. Som and T. Pradeep, *Acc. Chem. Res.*, 2017, **50**, 1988–1996.
- 18 Q. Yao, Z. Wu, Z. Liu, Y. Lin, X. Yuan and J. Xie, *Chem. Sci.*, 2021, **12**, 99–127.
- 19 X. Du and R. Jin, *ACS Nano*, 2019, **13**, 7383–7387.
- 20 Y. Du, H. Sheng, D. Astruc and M. Zhu, *Chem. Rev.*, 2019, **120**, 526–622.
- 21 Y. Li, S. Li, A. V. Nagarajan, Z. Liu, S. Nevins, Y. Song, G. Mpourmpakis and R. Jin, *J. Am. Chem. Soc.*, 2021, **143**, 11102–11108.
- 22 X.-R. Song, N. Goswami, H.-H. Yang and J. Xie, *Analyst*, 2016, **141**, 3126–3140.
- 23 C. G. Jones, M. W. Martynowycz, J. Hattne, T. J. Fulton, B. M. Stoltz, J. A. Rodriguez, H. M. Nelson and T. Gonen, *ACS Cent. Sci.*, 2018, **4**, 1587–1592.
- 24 M. Azubel, J. Koivisto, S. Malola, D. Bushnell, G. L. Hura, A. L. Koh, H. Tsunoyama, T. Tsukuda, M. Pettersson, H. Häkkinen and R. D. Kornberg, *Science*, 2014, **345**, 909–912.
- 25 M. Azubel, A. L. Koh, K. Koyasu, T. Tsukuda and R. D. Kornberg, *ACS Nano*, 2017, **11**, 11866–11871.
- 26 S. Vergara, D. A. Lukes, M. W. Martynowycz, U. Santiago, G. Plascencia-Villa, S. C. Weiss, M. J. de la Cruz, D. M. Black, M. M. Alvarez, X. López-Lozano, C. O. Barnes, G. Lin, H.-C. Weissker, R. L. Whetten, T. Gonen, M. J. Yacaman and G. Calero, *J. Phys. Chem. Lett.*, 2017, **8**, 5523–5530.
- 27 P. Ramasamy, S. Guha, E. S. Shibu, T. S. Sreepasad, S. Bag, A. Banerjee and T. Pradeep, *J. Mater. Chem.*, 2009, **19**, 8456–8462.
- 28 A. Nag, P. Chakraborty, M. Bodiuzzaman, T. Ahuja, S. Antharjanam and T. Pradeep, *Nanoscale*, 2018, **10**, 9851–9855.